

# Microstructural influences on crack initiation and growth in an equiatomic NiTi PE alloy

F. Iacoviello<sup>1</sup>, V. Di Cocco<sup>1</sup>, S. Natali<sup>2</sup> and C. Maletta<sup>3</sup>

<sup>1</sup> University of Cassino, Di.M.S.A.T., via G. Di Biasio 43, 03043 Cassino (FR), Italy, v.dicocco@unicas.it

<sup>2</sup> University of Rome "Sapienza", Dip.I.C.M.A., Via Eudossiana 18, Rome, Italy.

<sup>3</sup> University of Calabria", Dept. Mech. Eng., 87036 Rende (CS), Italy.

**ABSTRACT.** *In this work the stress-induced microstructural transitions and the crack initiation and growth mechanisms in a near equiatomic NiTi shape memory alloy have been analyzed, by XRD and SEM investigations. In particular, miniaturized dog-bone shaped specimens and a special testing machine have been used which allow in situ XRD and SEM investigations during mechanical loading, at fixed values of the applied deformation. Direct and reverse stress-induced phase transition mechanisms, between the parent austenitic phase and the product martensitic one, have been captured by X-Ray diffraction tests while the crack initiation and propagation have been observed by scanning electron microscopy. These analyses revealed that stress-induced transformations, from austenite to martensite, occurs near the crack tip, as a consequence of the highly localized stress, which significantly affects the crack propagation mechanisms with respect to common metals. In fact, blunting does not occurs during mechanical loading and, in addition, complete crack closure is observed during unloading, as a consequence of the reverse transformation from product to parent phase.*

## INTRODUCTION

Shape memory alloys (SMAs) are an important class of materials which exhibit unique features with respect to common metallic alloys, such as the shape memory effect (SME) and pseudo-elastic effect (PE). In particular, due to these properties SMAs are able to recover their original shape after being mechanically deformed to a large extent, by heating up to a characteristic temperature (SME), or by removing the mechanical load (PE). From the microstructural point of view shape memory and pseudoelastic effects are due to reversible solid state microstructural transitions from the high temperature parent austenitic phase to the low temperature product martensitic one. In particular, the phase transition can be activated by a temperature change (TIM, Thermally Induced Martensite), between the characteristic phase transition temperature, or by external mechanical loads (SIM, Stress Induced Martensite) [1 - 4].

Among these alloys, the near equiatomic NiTi binary system shows the most exploitable characteristics and it is currently used in an increasing number of applications in many fields of engineering [1, 6], for the realization of smart sensors and actuators, joining devices, hydraulic and pneumatic valves, release/separation systems, consumer applications and commercial gadgets. However, due to their good mechanical properties and biocompatibility the most important applications of NiTi alloys are in the field of medicine, where pseudoelasticity is mainly exploited for the realization of several components, such as cardiovascular stent, embolic protection filters, orthopedic components, orthodontic wires, micro surgical and endoscopic devices [7].

In any case, due to their interesting features and the efforts of many researchers the use of NiTi alloys is expected to rise considerably in the near future, even in low cost applications, due to a continuous improvement in product quality and cost reduction [8, 9].

In this work the mechanical properties of a commercial NiTi shape memory alloy have been investigated by tensile tests of miniaturized dog bone shaped specimens carried out by using a special mini testing machine, which allows in situ XRD and SEM investigations during mechanical loading. In particular, XRD analyses have been carried out at fixed values of the applied deformation, and the direct stress induced phase transformation (SIM) has been observed during loading together with the reverse transformation after unloading. Furthermore, in situ SEM investigations have been carried out to analyze the crack formation and growth. These analyses revealed that stress-induced transformations, from austenite to martensite, occurs near the crack tip, as a consequence of the highly localized stress, which significantly affects the crack propagation mechanisms with respect to common metals. In fact, blunting does not occur during mechanical loading and, in addition, complete crack closure is observed during unloading, as a consequence of the reverse transformation from product to parent phase.

## **MATERIAL AND EXPERIMENTAL METHODS**

A commercial pseudo-elastic NiTi alloy (Type S, Memory metallo, Germany), with nominal chemical composition of 50.8at.% Ni - 49.2 at.% Ti, was used in this investigation. In Fig. 1 light micrographs of the initial austenitic microstructure of the alloy are illustrated at different magnification, which shows the presence of inclusions and subgrains. This is an expected result as the inclusions play a significant role in the stress-induced phase transformation mechanisms and, consequently, in the macroscopic pseudo-elastic response of the alloy. The isothermal engineering stress-strain curve of the material at room temperature ( $T=298$  K) is illustrated in Fig. 2.a, together with the values of the main mechanical parameters of the alloy, *i.e.* the Young's moduli of austenite ( $E_A$ ) and martensite ( $E_M$ ), the uniaxial transformation stress ( $\sigma_{tr}$ ) and transformation strain ( $\epsilon_L$ ).

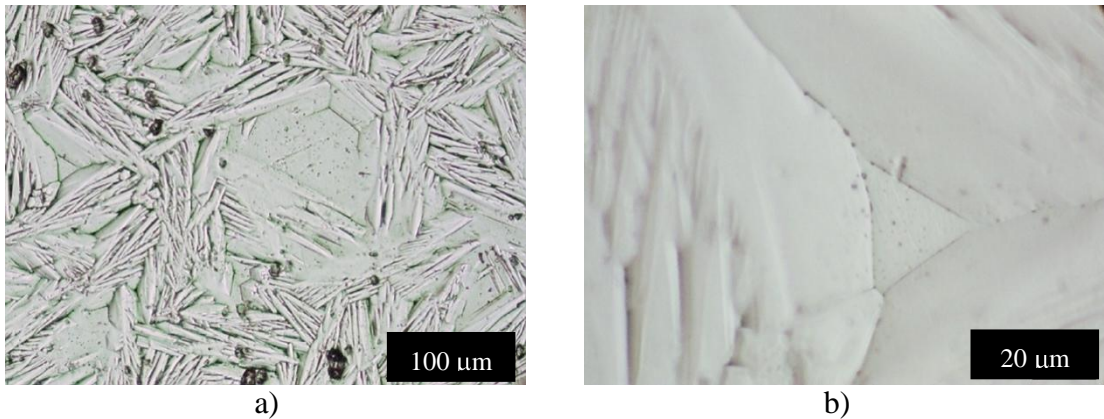


Figure 1: Initial austenitic microstructure of the alloy: a) at low magnification showing the presence of inclusions, b) high magnification with presence of subgrains.

The evolution of the microstructure during uniaxial deformation was analyzed by using miniature dog-bone shape specimens, shown in Fig. 2.b, and a special testing machine which allows *in-situ* scanning electron microscopic (SEM) observations as well as X-Ray diffraction (XRD) analyses. In particular, the testing machine is equipped with a removable loading frame, which allows SEM and X-Ray analyses at fixed values of applied load and/or deformations. The specimens were machined from commercial NiTi sheets with thickness  $t=0.5$  mm, by wire electro discharge machining, due to the poor workability of this class of materials by conventional machining processes as well as to reduce the formation of thermo-mechanical affected zone.

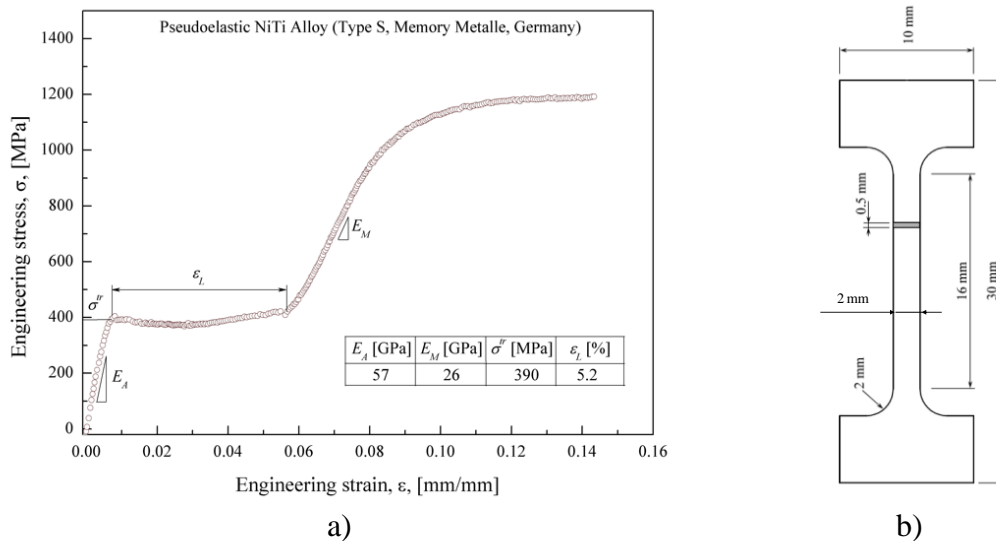


Figure 2: a) Isothermal stress-strain curve of the alloy ( $T=298K$ ); b) miniature dog-bone shaped specimen.

Step by step isothermal tensile tests were carried out, at room temperature, at increasing values of the specimen elongation. In particular, three levels of elongation

have been applied,  $\delta=0.8, 1.6$  and  $2.4$  mm, which can be expressed as gross engineering strain ( $\epsilon_g$ ) with respect to the gauge length  $L_0=16$  mm, *i.e.*  $\epsilon_g=5, 10$  and  $15\%$ . In particular, for each loading step the loading frame containing the specimen was removed from the testing machine, at fixed values of deformation, and XRD measurements and SEM observations were carried out. In particular, XRD tests were carried out by using a Philips X-PERT diffractometer equipped with a vertical Bragg–Brentano powder goniometer. A step–scan mode was used in the  $2\theta$  range from  $30^\circ$  to  $90^\circ$  with a step width of  $0.02^\circ$  and a counting time of 2 s per step. The employed radiation was monochromated  $\text{CuK}\alpha$  (40 kV – 40 mA). The calculation of theoretical diffractograms and the generation of structure models were performed using the PowderCell software. SEM investigations were carried out with the aim of capturing both phase transition mechanisms and the formation and propagation of cracks during mechanical loading.

## RESULTS AND DISCUSSION

### *Finite element analysis*

Preliminary numerical simulations, by using a commercial finite element software, were carried out in order to correlate the gross engineering strain ( $\epsilon_g$ ), measured by the miniature testing machine, to the effective engineering strain ( $\epsilon_e$ ), *i.e.* to the experimentally measured engineering stress-strain curve of Fig. 2.a. To this aim a 2D FE model was made to simulate the testing conditions of the miniature specimen, and a standard non-linear solutions were adopted to model the complex stress strain behavior of the material illustrated in Fig 2.a. In particular, a quarter of the miniature specimen was modeled, due to symmetric geometry and boundary conditions, together with a part of the loading frame, and contact conditions were defined between them in order to simulate, as close as possible, the real testing conditions. Fig. 3.a illustrates the FE mesh which consists of about 800 4-noded plane stress quadrilateral elements while Fig. 3.b shows a comparison between the numerically simulated stress-strain curve relative to net and gross engineering strain. This latter was calculated from the displacement of the specimen head, according to the experimental conditions. As expected, gross strain is significantly greater than net strain and the difference increases when increasing the applied stress. This effect can be attributed to two different mechanisms: the compliance of the miniaturized testing machine and the deformation on the specimen heads. Note that a linear correction of the gross strain cannot be used here as the material non-linearity causes a marked non-linear relation between gross and net strain. For a better understanding of the results reported in the following section Fig. 3.b illustrates the relation between gross strain and net strain within the range of deformation of the experiments.

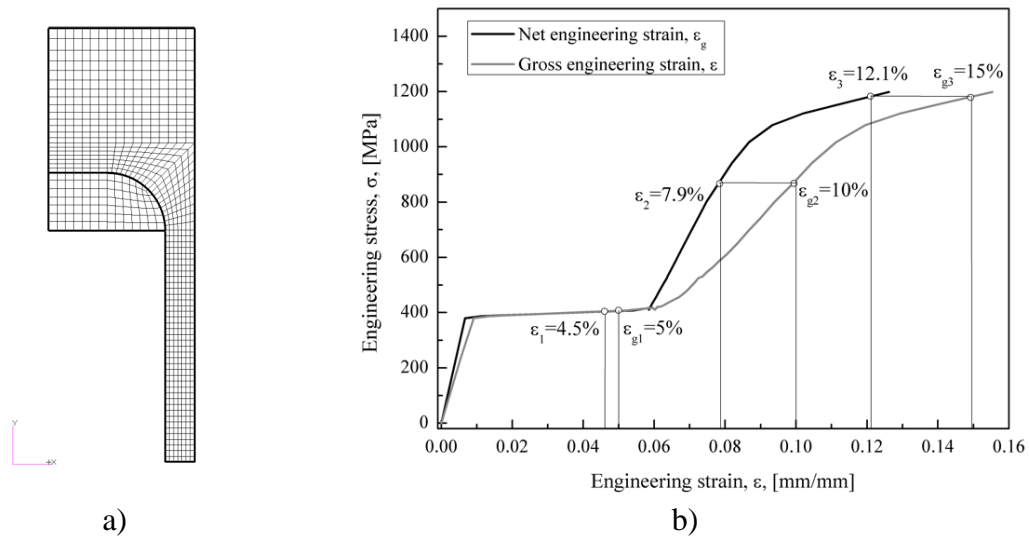


Figure 3: FE analysis of the testing condition: a) FE model of the specimen and b) relation between gross and net engineering strain obtained from FE simulations.

### X-Ray diffraction Analyses

The first X-Ray diffraction test was carried out under undeformed conditions and the obtained spectrum is illustrated in Fig.4. The figure shows two peaks at  $42.39^\circ$  and  $77.54^\circ$ , which correspond to [011] and [022] crystallographic planes, typical of the austenitic phase. The two peaks have been used to evaluate the cell parameter equal to about  $3.012 \text{ \AA}$ .

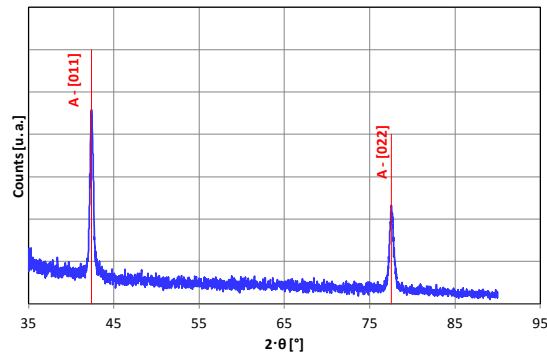


Figure 4: X-Ray spectrum of the investigated NiTi alloy in stress free condition.

At the gross engineering strain  $\varepsilon_g=5\%$ , corresponding to the effective engineering strain  $\varepsilon_e=4.5\%$  and to a stress  $\sigma=400 \text{ MPa}$  (See Fig. 3.b), three new peaks have been observed ( $42.99^\circ$ ,  $78.17^\circ$  and  $80.29^\circ$ ), as illustrated in Fig. 5.a. These new peaks revealed the presence of the martensite phase which is obtained on the stress plateau of the  $\sigma$ - $\varepsilon$  curve.

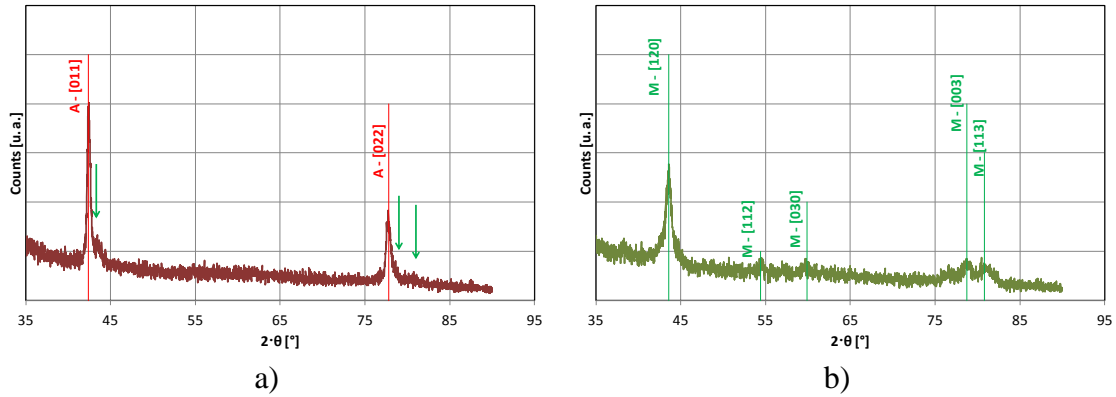


Figure 5: X-Ray spectra of the investigated NiTi alloy: a) at  $\varepsilon_g=5\%$ ; b) at  $\varepsilon_g=10\%$ .

Evidence of phase transition is confirmed when increasing the gross deformation up to  $\varepsilon_g=10\%$ , corresponding to the effective engineering strain  $\varepsilon_e=7.9\%$  and to a stress of about  $\sigma=800$  MPa; this loading condition corresponds to the fully transformed martensitic structure as illustrated in Fig. 3.b. In this case the new phases are completely developed and their spectra are illustrated in Fig. 5.b, where five peaks are observed corresponding to a monoclinic phase characterized by three cell parameters of about  $a=b=3.800$  Å,  $c=2.600$  Å and  $\alpha=80^\circ$ . The Miller indexes of the three peaks are shown in Tab. 1.

Table1: Miller plane indexes and corresponding peak angles.

[120]	[112]	[030]	[003]	[113]
43.55°	54.39°	59.90°	78.72°	80.80°

### SEM analyses

Figures 6 show SEM observations of a lateral crack within the gauge length of one of the test specimen, which initiated from a machining flaw. In particular, the dark gray arrows indicate the evolution of the main crack during mechanical loading while the white arrows show other secondary micro cracks. The main crack was observed under the applied gross engineering strain  $\varepsilon_g=10\%$  (Fig. 6.a) and the evolution was analysed with increasing the applied deformation for  $\varepsilon_g=11\%$  (Fig. 6.b),  $\varepsilon_g=12\%$  (Fig. 6.c) up to complete failure of the specimen (Fig. 6.d), which occurs elsewhere. The figure clearly show an increase of the crack tip opening displacement with increasing the applied deformation; however, a negligible blunting is observed, likely attributed to the formation of stress-induced martensite in front of the tip. The stress-induced transformation mechanism and its reversion, from martensite to austenite, is also confirmed by the nearly complete crack closure after failure (Fig. 6.d), which indicates a great recovery capability due to the pseudoelastic properties of the alloy. This recovery mechanism was also observed in the secondary micro cracks (see white arrows in Figs. 6) as well in other lateral cracks, as shown in Fig. 7. This figures also show microstructure changes (see arrows in Fig. 7) in the crack tip field which indicate morphology modifications.

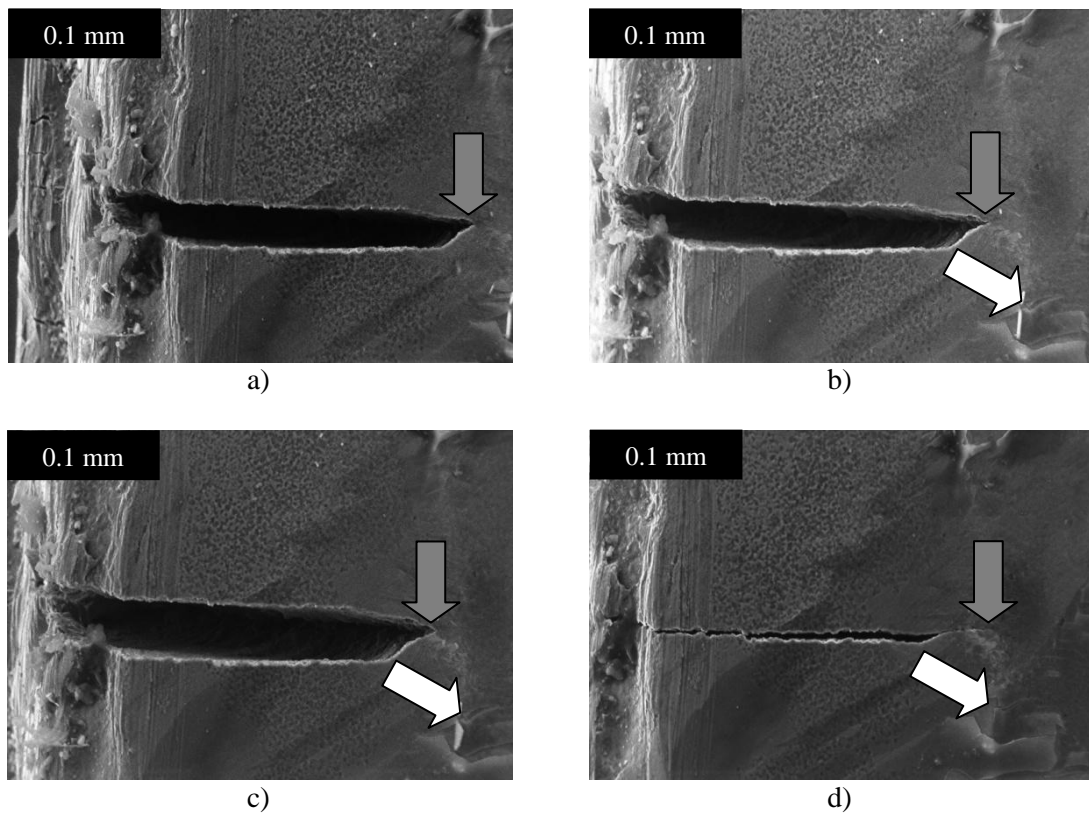


Figure 6: Lateral crack in the gauge length of the specimen under different values of applied deformation: a)  $\varepsilon_g=10\%$ , b)  $\varepsilon_g=11\%$ , c)  $\varepsilon_g=12\%$ , d) specimen failure.

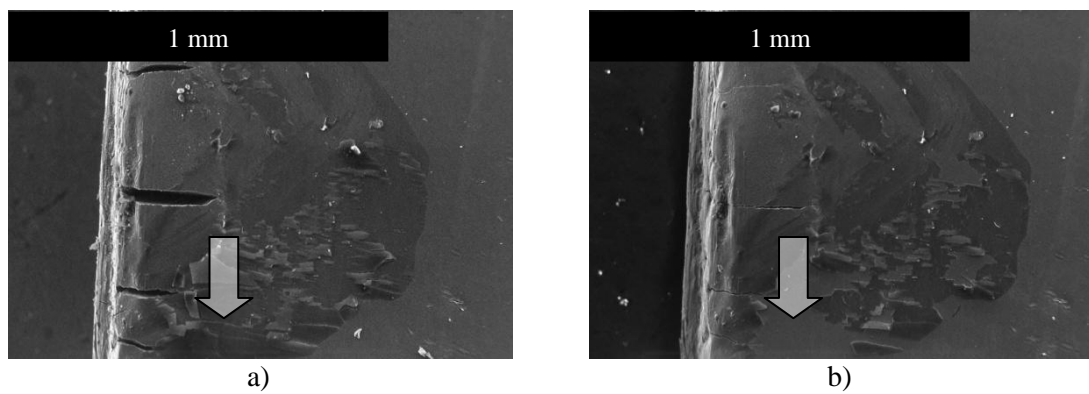


Figure 7: Multiple lateral cracks and microstructural changes near the cracks tip: a)  $\varepsilon_g=12\%$ , b) specimen failure.

## CONCLUSION

In this work a pseudoelastic NiTi shape memory alloy has been investigated by using a miniature testing machine, which allows *in-situ* scanning electron microscopic (SEM) observations and X-Ray diffraction (XRD) analyses. In particular, miniaturized uniaxial specimens were used and the micro-structure evolution, at increasing values of applied deformations, was analyzed together with the crack initiation and growth mechanisms. The results can be summarized as follows:

- an initial cubic structure, with cell parameter of about 3.012 Å, characterizes the investigated alloy in stress free conditions; at  $\varepsilon=4.5\%$ , corresponding to about  $\sigma=400$  MPa in the stress plateau of the  $\sigma$ - $\varepsilon$  curve, a new phase, the martensitic one, is observed; as well known the stress plateau is attributed to the transition from initial cubic structure to the new structure; at  $\varepsilon=7.9\%$ , corresponding to about  $\sigma=800$  MPa in the fully martensitic region of the  $\sigma$ - $\varepsilon$  curve, the new structure is completely developed and the initial structure is not observed. The new structure is characterized by monoclinic cells with three cell parameters of about  $a=b=3.800$  Å,  $c=2.600$  Å and  $\alpha=80^\circ$ ;
- A negligible crack tip blunting is observed which can be attributed to the formation of stress-induced martensite in front of the tip. Furthermore, the stress-induced transformation mechanism and its reversion, from martensite to austenite, is also confirmed by the nearly complete crack closure after failure, which indicates a great recovery capability due to the pseudoelastic properties of the alloy. Evidence of microstructural modifications in the crack tip region are also confirmed by morphology modifications.

## REFERENCES

1. Y. Liu, G.S. Tan., *Intermetallics* (2000) 8.
2. Y. Liu, D. Favier, *Acta Mater* (2000) 48.
3. S. Miyazaki, M. Kimura In: Otsuka K, Fukai Y, editors. *Advance materials* \_93, V/B: Shape memory materials hydrides. Amsterdam: Elsevier (1994) 1101.
4. A. Sato, E. Chishima, K. Soma, T. Mori, *Acta Metall* (1982);30:1177.
5. K. Otsuka Shimizu, *Scripta Metall* 1977;11:757.
6. Otsuka, K., Ren, X. (2005) *Progress in Materials Science* 511.
7. Dong, Y., Boming, Z., Jun, L. (2008) **485** *Materials Science and Engineering A*, 243–250.
8. K.C. Russel, *Phase transformation*, Ohio, ASM (1969) 1219.
9. *Shape memory materials hydrides*. Amsterdam: Elsevier; 1994. p. 1097.